

Organic & Biomolecular Chemistry

Accepted Manuscript

This article can be cited before page numbers have been issued, to do this please use: D. Maiti, A. S. M. Islam, M. Sasmal, A. Dutta, A. Katarkar and M. Ali, *Org. Biomol. Chem.*, 2020, DOI: 10.1039/D0OB00567C.



This is an Accepted Manuscript, which has been through the Royal Society of Chemistry peer review process and has been accepted for publication.

Accepted Manuscripts are published online shortly after acceptance, before technical editing, formatting and proof reading. Using this free service, authors can make their results available to the community, in citable form, before we publish the edited article. We will replace this Accepted Manuscript with the edited and formatted Advance Article as soon as it is available.

You can find more information about Accepted Manuscripts in the [Information for Authors](#).

Please note that technical editing may introduce minor changes to the text and/or graphics, which may alter content. The journal's standard [Terms & Conditions](#) and the [Ethical guidelines](#) still apply. In no event shall the Royal Society of Chemistry be held responsible for any errors or omissions in this Accepted Manuscript or any consequences arising from the use of any information it contains.

ARTICLE

A Coumarin Embedded Highly Sensitive Nitric Oxide Fluorescent Sensor: Kinetic Assay and Bio-imaging Applications

Debjani Maiti^a, Abu Saleh Musha Islam^a, Mihir Sasmal^a, Ananya Dutta^a, Atul Katarkar^b, and Mahammad Ali^{*a,c}

Received 00th January 20xx,
Accepted 00th January 20xx

DOI: 10.1039/x0xx00000x

Abstract: Fluorescence spectroscopy is a significant bio-analytical technique for specific detection of Nitric Oxide (NO) and to broadcast the *in vitro* and *in vivo* biological activities of this gasotransmitter. Herein, a benzo-coumarin embedded smart molecular probe (BCM) is employed for NO sensing through detailed fluorescence studies in purely aqueous medium. All the Spectroscopic analysis and literature reports clearly validate the mechanistic insight of this sensing strategy i.e., the initial formation of 1,2,3,4-oxatriazole on treatment of the probe with NO which finally converted to its carboxylic acid derivative. This oxatriazole formation consequences a drastic enhancement in fluorescence intensity due to PET effect. The kinetic investigation unveils the second and first-order dependency on [NO] and [BCM] respectively. The very low detection limit (16 nM), high fluorescence enhancement (123 fold) in aqueous medium and good formation constant ($K_f = (4.33 \pm 0.48) \times 10^4 \text{ M}^{-1}$) along with pH invariability, non-cytotoxicity, biocompatibility and cell permeability recognise this probe as very effective one for tracking of NO intracellularly.

Introduction

For a few decades, biologically abundant reactive nitrogen species (RNS) have exposed their pivotal roles as a cell signalling molecule in the course of diverse physiological and pathological processes.¹ Nitric Oxide (NO), a prime member of this class is a pervasive gasotransmitter and associated with numerous physiological processes in many bio-organisms. Endogenous production of NO takes place through the conversion of L-arginine to L-citrulline which is catalysed by eNOS, nNOS and iNOS (NO synthase enzymes).² Physiologically, NO functions as (i) stimulator in vascular smooth muscle relaxation, (ii) prevents infections functioning on immune system and (iii) serves itself as neurotransmitter.^{3,4} The pathological impact in malfunctioning of NO homeostasis is incorporated with carcinogenesis, neurodegenerative injury, endothelial dysfunction, diabetes, chronic liver inflammation etc.^{5,6} Nitric oxide is involved in the modulation of gene transcription and acts as a controlling factor in the translation of *m*-RNA.^{7,8} Considering all these unambiguous significance of this bio-regulatory molecule, several methods like chemi-luminescence, electrochemistry, colorimetric assay, electron-paramagnetic resonance spectroscopy, fluorimetric techniques⁹⁻¹⁴ etc. are widely used to comprehend the NO biology.

But among these analytical methods, fluorescence technique is concerned as a most conducive one for endogenous NO detection owing to its high sensitivity, non-destructive and real-time imaging properties, minimal invasiveness, sophisticated instrumentations and high spatio-temporal resolution.¹⁵⁻¹⁹ Thereby, exploiting the fluorescence spectroscopic technique a plenty of nitric oxide probes has been emerged: i) organic probes ii) single-walled nano tube (SWNT) probes iii) quantum dots (QD) probes iv) metal complex based probes.²⁰⁻²⁷ The *o*-phenylene diamine (OPD) moiety, in the class of organic probe, is one of the promising receptor for NO leading to the formation of triazole with a significant enhancement of fluorescence intensity.²⁰⁻³³ Though this strategy dragged a deep attention of researchers, still its applications are limited by some serious shortcomings. As for examples, (a) the vicinal diamine may suffer from oxidation by various oxidants present in biological system, (b) the triazole formed in the reaction with NO may display different fluorescence response at different pH due to the presence of secondary –NH group, which may lead to misinterpretation of fluorescence data.^{30,31,33} Considering all these limitations, our group has disclosed a novel strategy for nitric oxide sensing by embedding quinoline as a fluorophore moiety which is flanked by acyl hydrazide group. Upon treatment with nitric oxide this probe primarily forms 1,2,3,4 oxatriazole causing a substantial enhancement in fluorescence intensity³⁴ which finally converted to carboxylic acid.³⁴ In our present work, we have used coumarin as a fluorophore which is planar, rigid and pi-conjugated heterocycle. For a few decades it was pretty recognized that active site at 3 position of coumarin with its benzo counterpart are strongly fluorescent.³⁵ It is a naturally occurring organic compound found in plants and oil, like oil of cassia, sweet

^a Department of Chemistry Jadavpur University, Kolkata 700 032, India; Fax: 91-33-2414-6223, E-mail: m_ali2062@yahoo.com, mali@chemistry.jdvu.ac.in

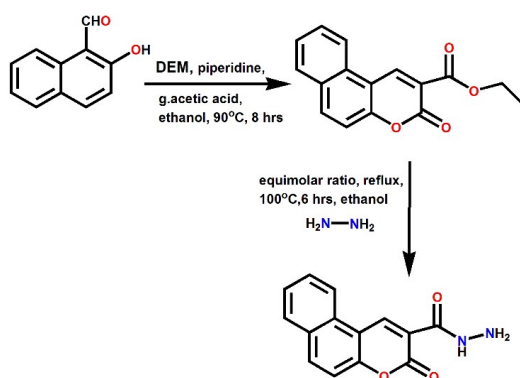
^b Department of Biochemistry, University of Lausanne, Ch. des Boveresses 155, 1066 Epalinges, Switzerland

^c Vice-Chancellor, Aliah University, II-A/27, Action Area II, Newtown, Action Area II, Kolkata, West Bengal 700160; vc_au@aliah.ac.in

clover, woodruff, tonka beans and lavender. Coumarin derivatives are well recognized due to their plenty of activities in pharmaceuticals, insecticides, agrochemicals, fragrances, polymer sciences and also identified as an important organic fluorescent materials.³⁶ It is also used in the treatment of burns, brucellosis, rheumatic disease, etc.³⁷ In respect to photophysical activities, coumarin and its derivatives exhibit high photostability, easy synthesis, extended spectral range and good solubility³⁸⁻⁴⁰. So, considering all the significance, we developed our pioneering strategy by using coumarin fluorophore joined with benzo- counter part which is synthesized by well-known Knoevenagel condensation followed by hydrazination. Herein, the relevant studies to comprehend the selectivity and sensitivity of BCM towards NO with plausible mechanism has been performed in terms of concentration and time dependent manner along with detailed cell imaging applications and theoretical studies. In addition, very high sensitivity to nitric oxide with 123 fold fluorescence enhancement in purely aqueous medium under physiological pH, very low detection limit (16nM) has been observed which increases efficacy of the probe for NO detection.

Results and discussion

Scheme-1 displays two steps synthetic pathway for the synthesis of 3-Oxo-3H-benzo[f]chromene-2-carboxylic acid hydrazide, (hereafter designated as BCM). The first step is a very well-known Knoevenagel condensation between 2-hydroxy naphthaldehyde and di-ethyl malonate in the presence of piperidine and glacial acetic under refluxing condition. After 8 h, the reaction mixture is cooled to room temperature whereupon pure product (L¹) was formed which was collected by filtration and well analyzed by ¹H NMR (Fig. S1), ¹³C NMR (Fig. S2).



Scheme 1. Synthetic Pathway for the Probe BCM.

The second step comprises the treatment of corresponding ester with hydrazine hydrate in equimolar ratio. The targeted fluorescent probe was well characterized by common spectroscopic studies, i.e., ¹H NMR (Fig. S3), ¹³C NMR (Fig. S4), mass spectrum (Fig. S5), and FTIR (Fig. S6). The receptor exhibits very high affinity and selectivity towards NO in aqueous medium.

Photophysical response of BCM towards NO

The fluorescence properties of the probe BCM and affinity towards nitric oxide were analyzed by performing the fluorescence titration **Fig.1**. For this experiment, a fixed concentration (20 μ M) of BCM was added in a cuvette containing 2.5 ml of aqueous HEPES buffer at 25 $^{\circ}$ C. Then, the NO solution was added progressively in the concentration range from 0 to 40 μ M. BCM alone exhibits very weak fluorescence in aqueous HEPES buffer whereas,

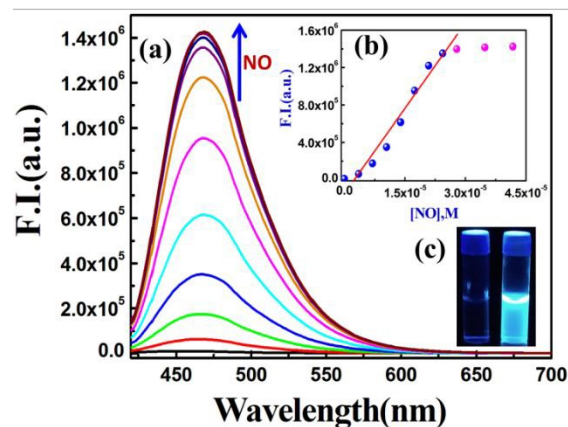


Fig.1. (a) Fluorescence emission spectra recorded taking only fixed 20 μ M BCM and also gradual addition of NO (0–40 μ M) at 25 $^{\circ}$ C in 10 mM HEPES buffer at pH 7.0, λ_{ex} = 410 nm and λ_{em} = 470 nm. (b) linear plot of F.I. vs. [NO]. (c) The image of probe BCM (left) and NO treated product (right) exposing in UV light.

gradual addition of NO causes a steady generation of fluorescence intensity resulting \sim 123 fold enhancement at λ_{em} \sim 470 nm (λ_{ex} = 410 nm). To determine the apparent formation constant we have carried out fluorescence titration experiment and a plot of F.I. vs. [NO], manifests an excellent linearity of the curve up to 25 μ M after which the plot gets saturated (maximum NO 40 μ M). The linear part was easily solved by utilizing the equation (1)⁴¹ under the condition $1 \gg cx^n$ and $n=1$.

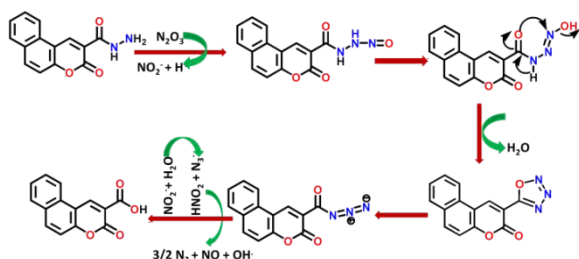
$$y = \frac{(a + b \times c \times x^n)}{1 + c \times x^n} \quad (1)$$

where, parameters a and b denote F.I. of the probe in the absence and presence of excess NO respectively, c is the formation constant designated as K_f . The slope ($b \times c$) obtained from the curve gives, $c = K_f = (4.33 \pm 0.48) \times 10^4 \text{ M}^{-1}$ (using b = F.I. in the presence of large excess NO).

Mechanistic view of fluorescence sensing of receptor BCM towards NO

To comprehend a neat and tidy insight into the mechanism which is responsible for fluorescence enhancement, we collected the product of the reaction between BCM and NO. For this purpose, BCM was dissolved (1 mmol, 0.254 g) in minimum volume of dichloromethane (DCM) and finally with 20 ml acetonitrile under aerobic condition. Then nitric oxide gas was bubbled through the probe solution for 15 minutes. A vivid fluorescence was noticed throughout the solution. Solvent was evaporated under pressure. The brown solid was

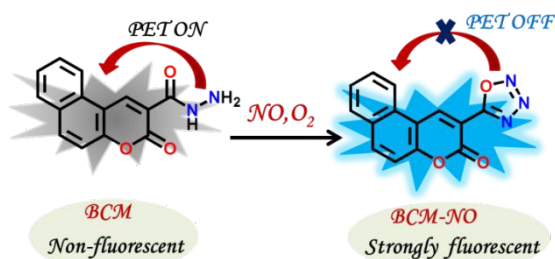
collected and further purified by recrystallization in ethanol. The pure crystalline compound was filtered and characterized by ESI-MS⁺ (Fig. S7), ¹H NMR (Fig. S8) and IR spectrometry (Fig. S9). The ESI-MS⁺ spectrum (Fig. S7) shows a peak at 304.0406 (1,2,3,4-oxatriazole + K⁺) suggesting the generation of 1,2,3,4-oxatriazole (BCM-NO) which was further assured by the abolishing of –NH (9.39 ppm) and –NH₂ (4.79 ppm) peaks in ¹H NMR spectra (Fig. S8). The generation of IR peak at 1600 cm⁻¹ (–N=N) and 1666 cm⁻¹ (–C=N) also strengthen the formation of oxatriazole moiety (Fig. S9).



Scheme 2. Possible Reaction Mechanism of BCM and NO.

The predicted mechanism is outlined in scheme-2, where NO first reacts with O₂ to generate N₂O₃ under aerobic condition which nitrosylates –NH₂ of BCM to generate –NH–NO which ultimately generates 1,2,3,4-oxatriazole (BCM-NO) as a stable product. The formation of such electron deficient oxatriazole moiety originates a large enhancement in fluorescence intensity at λ_{em} = 470 nm. It is interesting to note that the formed oxatriazole is finally transformed to carboxylic acid through the formation of azide after keeping it in solution for a long time and was assured by Mass spectra (Fig. S10), ¹H NMR spectrum (Fig. S11).

From the electronic point of view the main-stream mechanism for NO sensing by OPD based probes is based upon the PET block process.⁴²⁻⁴⁴ Very recently, our group reported a quinoline based NO sensor containing acyl hydrazide moiety where PET effect³⁴ was operative. In the current report, we propose that the PET-ON mechanism due to electron push from hydrazide part to the coumarin fluorophore makes the probe BCM as weakly fluorescent. However, upon reaction with NO a remarkable fluorescence enhancement has been perceived which may arise due to the generation of electron deficient 1,2,3,4-oxatriazole moiety that restricts the above PET-ON process (**scheme-3**).



Scheme 3. Pet Effect Responsible for NO Sensing.

Time dependent reaction of BCM with NO, a kinetic approach

To assure a clear view of the operative mechanism of reaction between BCM and NO, we have thoroughly performed kinetic studies at pH 7.0 (10 mM HEPES buffer, 0.10 M NaCl), 15 °C, under

pseudo-first-order conditions using fluorometric technique (Fig. 2). In this study, we have taken a fixed concentration of BCM (5 μM) and variable [NO] (20–100 μM). The kinetic traces at 470 nm unveil it as single exponential growth curves assigning the first-order dependency of reaction rate on [BCM]. The time dependent fluorescence study also shows the fluorescence intensities at 470 nm increases with time and reach a plateau within ~5 min (Fig. S12). The pseudo-first-order rate constants (*k*_{obs}) obtained from the growth curves have been plotted against [NO], which yields a nonlinear upward curvature.

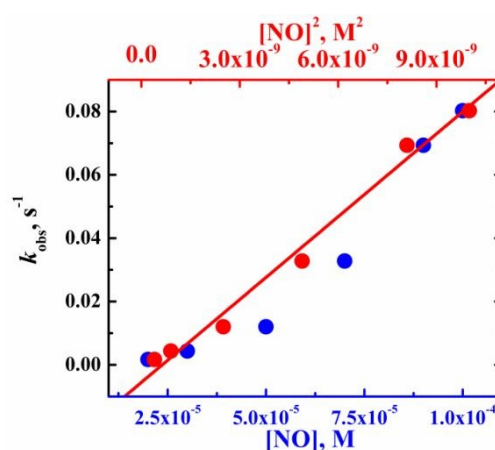
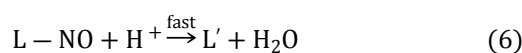
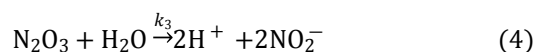


Fig. 2. The *k*_{obs} vs. [NO] plot gives an upward curvature (blue solid circles) while a plot of *k*_{obs} vs. [NO]² gives straight line (red solid circles). Experimental conditions are: [BCM] = 5 μM and [NO] = (20–100) μM, temperature = 15 °C in 10 mM HEPES buffer (pH = 7.0, NaCl = 0.10 M). All the data were collected using fluorescence technique.

However, a plot of *k*_{obs} vs. [NO]² displayed a well fitted straight line which delineates the second-order dependency upon [NO] (Fig. 2). The log(*k*_{obs}) vs. log[NO] plot furnishes a straight line with a slope = (2.42 ± 0.08) with R = 0.997 which also supports the second order kinetics with respect to [NO] (Fig. S13). We have accomplished a second experiment to evaluate the dependency of rate upon [BCM] taking a fixed 5 μM [NO] with variable [BCM] in the range between 20 and 100 μM. Here, a plot of log*k*_{obs} vs. log[BCM] clearly demonstrates a first-order dependence on [BCM] with slope = (1.19 ± 0.05) (Fig. S14) and R = 0.997.

Here, a provisional reaction sequence is formulated as follows:



The above reaction sequence clearly demonstrates that NO interacts firstly with its oxidized product NO₂ to form N₂O₃ that acts as a NO⁺ donor in the next step under aerobic condition. Then the formed N₂O₃ nitrosylates the amine hydrazide to generate L-NO which consequences the synthesis of a closed ring 1,2,3,4-oxatriazole moiety in a fast step (Scheme 2). We have surveyed the literature to afford the rate constants of the above-mentioned reactions as: $k_1 = 6.33 \times 10^6 \text{ M}^{-2} \text{ s}^{-1}$,⁴⁵ $k_2 = 1.1 \times 10^9 \text{ M}^{-1} \text{ s}^{-1}$,⁴⁶ and $k_3[\text{H}_2\text{O}] = 1.6 \times 10^3 \text{ s}^{-1}$.⁴⁷ With the knowledge of these rate constants we can stipulate that NO₂ and N₂O₃ are present in very negligible amount as reactive intermediates. By applying a steady-state approximation eqn. 7 can be attained for the formation of L' (BCM-NO).

$$\frac{d[\text{L}']}{dt} = \frac{k_1 k_4 [\text{L}]}{2(k_3[\text{H}_2\text{O}]) + k_4[\text{L}]} [\text{NO}]_t^2 [\text{O}_2]_t \quad (7)$$

From the previously illustrated kinetic studies, it was found that the reaction kinetics follows second and first order dependence with respect to [NO] and [L] ([BCM]) respectively which lead us to take an assumption that, $k_3[\text{H}_2\text{O}] \gg k_4[\text{L}]$. Now the eqn. 7 reduces to eqn. 8.

$$\frac{d[\text{L}']}{dt} = \frac{k_1 k_4 [\text{L}]}{2k_3[\text{H}_2\text{O}]} [\text{NO}]_t^2 [\text{O}_2]_t \quad (8)$$

As the kinetics was performed maintaining the pseudo-first-order conditions, taking L (BCM) as a minor component (the dissolved [O₂]_t = 2.5 mM at 25 °C) eqn. 8 reduces to eqn. 9, where $k_{\text{obs}} = \{d[\text{L}']/dt\}/[\text{L}]$

$$k_{\text{obs}} = k' [\text{NO}]_t^2 \quad (9)$$

taking,

$$k' = \frac{k_1 k_4}{2k_3[\text{H}_2\text{O}]} [\text{O}_2]_t \quad (10)$$

The value of k_4 is evaluated by utilizing the previously observed values of k_1 and $k_3[\text{H}_2\text{O}]$ mentioned above along with $k' = 8.60 \times 10^6 \text{ M}^{-2} \text{ s}^{-1}$, achieved from the linear plot of k_{obs} vs. [NO]² at 15 °C. From all of these data the value of k_4 was estimated to be $17.3 \times 10^5 \text{ M}^{-2} \text{ s}^{-1}$ and found to be very much similar in the order to some analogous reactions of N₂O₃ as follows: HSA ($0.3 \times 10^5 \text{ M}^{-1} \text{ s}^{-1}$), N-acetyl cysteine ($1.5 \times 10^5 \text{ M}^{-1} \text{ s}^{-1}$), GSH ($2.9 \times 10^5 \text{ M}^{-1} \text{ s}^{-1}$), Cys ($2.6 \times 10^5 \text{ M}^{-1} \text{ s}^{-1}$), BSA ($0.06 \times 10^5 \text{ M}^{-1} \text{ s}^{-1}$). Interestingly, this result is also in accord with our reported works.^{34,48}

Limit of detection

We have also performed the study to evaluate the detection limit of NO by BCM which reveals to be very low ~16 nM (Fig. S15) making the probe very sensitive towards NO in macrophage cultures,⁴⁹ where nitric oxide is present in micromolar to nanomolar range. So

the concerned NO probe (BCM) is highly applicable for monitoring NO quantitatively in these cell types. DOI: 10.1039/D0OB00567C

pH stability

To be an efficient fluorescent probe, it should show pH tolerance in the physiological range of pH so that it can be easily applicable in bio-organisms. For this purpose we have assessed the pH effect on photophysical behavior of BCM in the absence and presence of excess NO. Fig. 3 shows very high fluorescence intensity of the

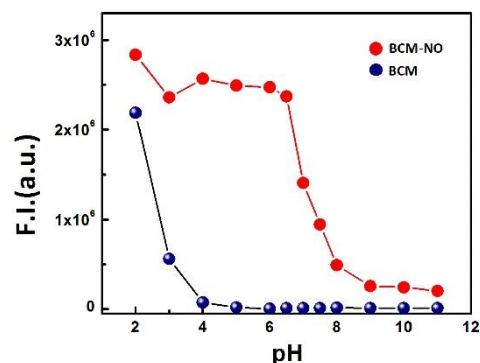


Fig. 3. pH dependent NO detection by BCM at 470nm $\lambda_{\text{ex}}=410\text{nm}$ at 25 °C in 10mM HEPES buffer.

probe and its NO treated product in low pH range (2-3). Probably the PET based probe BCM, due to presence of electron donor group (-NH-NH₂) is converted to its protonated form which would block the PET process generating the fluorescence intensity at lower pH range. In the pH range 4-8 the probe shows very weak fluorescence, however on treatment with NO it displays a drastic enhancement in fluorescence intensity due to oxatriazole formation. Moreover, at alkaline pH (> 8) the fluorescence intensity of NO treated product is inhibited likely due to rapid decomposition of N₂O₃ (eqn. 4), formed in the reaction of NO₂ and NO (eqn. 3) causing availability of lesser and lesser amount of reactive species (N₂O₃) towards the probe BCM (eqn. 5). Overall the pH study displays the well applicability of the probe at biological pH for tracing nitric oxide.

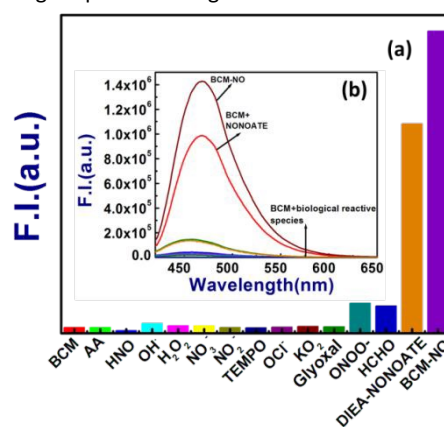


Fig. 4. (a) Bar plot represents the fluorescence responses of BCM at 470 nm ($\lambda_{\text{ex}} = 410 \text{ nm}$) towards various biological reactive species in HEPES buffer at pH 7.0, BCM = 20 μM , X²⁻ = 50 μM at 25 °C; (b) corresponding spectral responses.

Analyte selectivity experiment

The selectivity of a fluorescent probe towards a particular analyte is ensured by providing an appropriate binding site and some special chemical properties. Herein, the reactivity assay of probe BCM towards NO was conducted by using a broad array of putative interfering species like reactive species, important metal ions, and anions in 10 mM HEPES buffer, at 25°C at pH 7.0. Figs. S16 and S17, S18, S19 clearly manifest that BCM is silent in fluorescence response towards essential metal ions and anions. Likewise, the selectivity of BCM towards NO was ensured by reacting BCM with relevant biologically reactive species like H₂O₂, ClO⁻, KO₂, ⁻OH, NO, NO₂⁻, NO₃⁻, tempo, glyoxal, ONOO⁻, HNO, AA (ascorbic acid), HCHO which revealed none of these potential analyte triggered fluorescence enhancement, except NO (Fig. 4). To our delight, the important cellular metabolites like AA, glyoxal, HCHO interacts hardly with the concerning probe. So, this high selectivity is very much advantageous for precise detection of NO in biological milieu.

Geometry optimization with electronic structure

To get a theoretical overview on the interaction between BCM and NO we have conducted the DFT and TDDFT calculations of probe (BCM) and its NO mediated product (BCM-NO). Fig. 5 represents the optimized geometry of both the compounds having C₁ point group. The structural compositions of these compounds have been established using mass spectroscopy which denotes the formation of oxatriazole from carbohydrazide in the presence of NO. All the important geometrical parameters of the probe BCM and BCM-NO are tabulated in Table S1 and S2. For BCM-NO product N-O bond distance is 1.43 Å, whereas the C-O bond distances lie in the range of 1.2-1.4 Å.

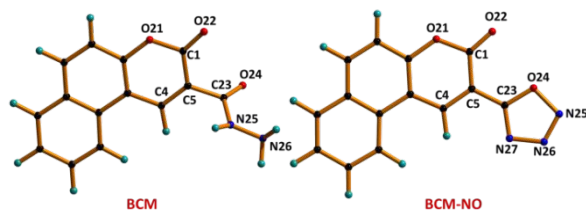


Fig. 5. Optimized geometry of BCM and BCM-NO.

In ground state the density of electron clouds mainly prevails on HOMO and LUMO molecular orbitals of the 3-Oxo-3H-benzo[f]chromene-2-carbaldehyde and 3-Oxo-3H-benzo[f]chromene-2-carboxylic acid amide moiety respectively in the probe BCM. In case of BCM-NO, the electron clouds mainly resides on HOMO and LUMO molecular orbital of the Benzo[f]chromen-3-one and 3-[1,2,3,4]Oxatriazol-5-yl-chromen-2-one moiety respectively (Fig. S20). These compositions are important to know the behaviour of the transition as well as the absorption spectra of both BCM and BCM-NO. The calculated HOMO-LUMO energy gap associated with BCM and BCM-NO is 3.94eV and 3.47eV respectively (Fig. 6). By exploiting TDDFT method, the UV-Vis absorption spectra of BCM and

BCM-NO were obtained at room temperature in aqueous medium (Fig. S21). The absorption band of BCM at 374 nm in pure aqueous medium corresponds to the peak at 354 nm (Fig. S20) obtained from the TDDFT calculation which is assigned to the S₀→ S₁ electronic transitions with significant oscillator strength (Table S3 and S4). Whereas, for BCM-NO the theoretically evaluated absorption band at 407 nm ascribed to the peak at 386 nm also associated with S₀→ S₁ electronic transitions (Fig. S20). So, from this information it can be speculated that the experimental results have good agreement with the theoretical ones.

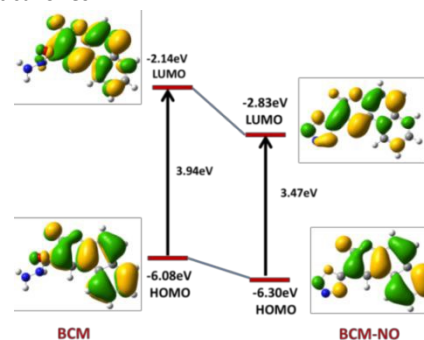


Fig. 6. Frontier molecular orbitals of probe BCM and BCM-NO.

NO Detection in Live Cells

The fluorescence imaging studies were executed to explore the detecting capability of BCM as NO sensors in living cell. The probe's cytotoxicity has been assessed in A375 and Raw 264.7 cells (Fig. 7). The cell lines showed evidence of well admissibility of BCM (more than 80% of the cell is viable upto 60 μM of BCM), indicating

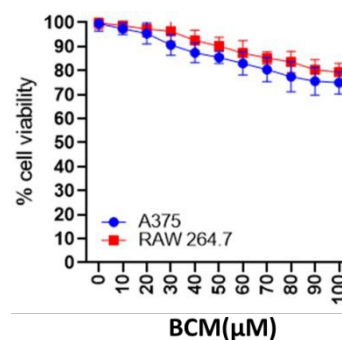


Fig. 7. Graphical picture of Cell viability study of BCM.

its effectiveness as NO sensor in live cells also. Exogenously stimulated NO sensing practicability of BCM was measured in A375 cells. The live cells were treated with NO donor DEA-NONOate followed by incubation with probe. BCM-NO showed intracellular fluorescence compared to BCM probe only (Fig. 8). Likewise, endogenously stimulated NO sensing of BCM probe has been estimated in Raw 264.7 cells where, the cells were treated with LPS (1.0 mg/mL) and IFN-γ (1000 U/mL) for 6h and then treatment with probe BCM (Fig. 9). Very obviously, in the presence of NO stimulator the cells exhibited high fluorescence compared to the non-stimulated and PTIO (NO scavenger) treated ones.

ARTICLE

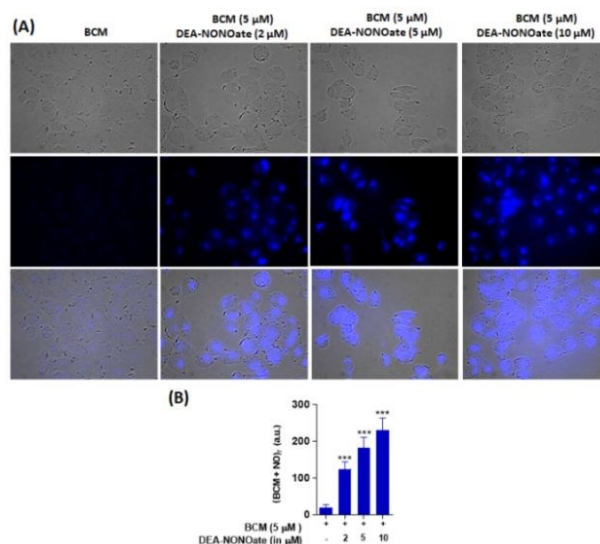


Fig. 8: (A) Images of A375 cells incubated with 5 μM BCM for 30 min and then incubated with DEA-NONOate (2, 5 and 10 μM) for 30 min. The blue fluorescence was observed owing to reaction of NO with BCM. Images were captured at 63X objective. (B) Quantification of fluorescence intensity in response to intracellular NO interaction with BCM.

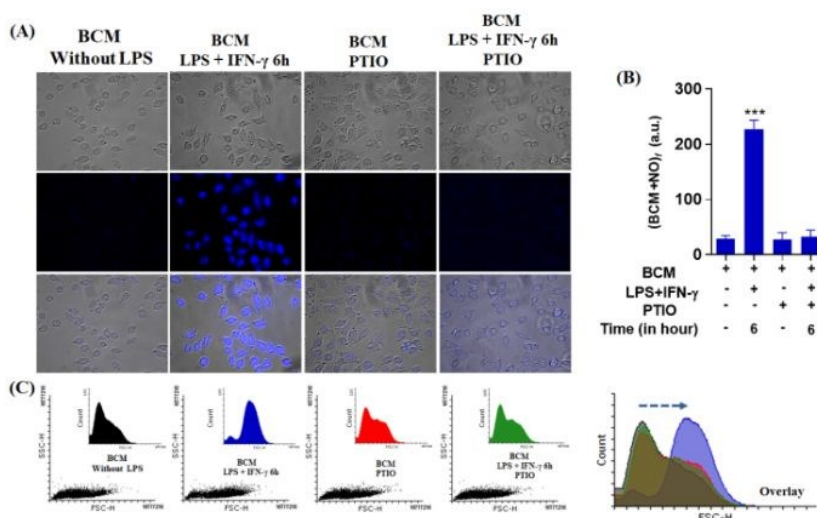


Fig. 9: Endogenous recognition of NO with flow cytometry assay: (A) Fluorescence images of Raw 264.7 macrophage cells incubated with BCM in the absence of LPS and stimulated with LPS+IFN- γ for 6h followed by the addition of PTIO, a NO scavenger. Corresponding images were captured at 63X objective. (B) The characteristic bar plots display the changes in fluorescence intensity of BCM upon interaction with LPS+IFN- γ , PTIO and LPS+IFN- γ +PTIO, respectively. The experiments were performed thrice and related data are represented as mean \pm SD. For statistical importance the estimated results were verified with the student's t test. P value \leq 0.05 were statistically significant. (C) Flow cytometry experiment of NO with BCM by taking the Flowing Software version 2.5.1. The representative dot plot of forward (FSC-H) versus

side (SSC-H) scatter and the corresponding histogram plot displaying a positive response for gated Raw 264.7 macrophage cells towards NO. The overlap histogram plot indicates a positive shift in fluorescence intensity peak of LPS+IFN- γ stimulated NO taken by BCM compared to without LPS+IFN- γ and PTIO.

Additionally, the Flow cytometric studies were performed in Raw 264.7 cells for the evaluation of NO, showing a positive shift in fluorescence peak for LPS+IFN- γ stimulated cells in contrast to the non-stimulated cells and PTIO (200 mM) (Fig. 9C). So finally it can be concluded that, BCM showed an excellent nontoxic fluorescence response towards NO for the purpose of cell imaging exogenously and endogenously.

EXPERIMENTAL SECTION

Materials. The reagents like 2-Hydroxy-1-naphthaldehyde, diethyl-malonate, piperidine, glacial acetic acid, hydrazine hydrate are of reagent grade and purchased from Sigma Aldrich. The sodium salts of anions, salts of metal ions (Pb²⁺, Mn²⁺, Co²⁺, Ni²⁺, Zn²⁺, Cu²⁺, Al³⁺, Hg²⁺, Mg²⁺, Fe³⁺, La³⁺, Cr³⁺ and Cd²⁺) and biological reactive species (H₂O₂, O²⁻, TEMPO radical, NO₃⁻, NO₂⁻, ClO⁻, AA, NO⁺, DEA-NONOate (sodium salt) were obtained either from Sigma-Aldrich or from other commercial suppliers and used without further purification. Solvents like DMF, MeCN, etc., (Merck, India) were of reagent grade and dried using standard methods.

Synthesis of ligand

The ligand 3-Oxo-3H-benzo[f]chromene-2-carboxylic acid hydrazide (designated as BCM) was synthesized by two step easy procedures.

Step-1: Synthesis of 3-Oxo-3H-benzo[f]chromene-2-carboxylic acid ethyl ester

2-Hydroxy-1-naphthaldehyde (10 mmol, 1.72 g), di-ethyl malonate (20 mmol, 3.2 g) is mixed in a round bottom flask in 20 ml ethanol under heating and stirring condition in presence of 1ml piperidine and 2 drops of glacial acetic acid. This reflux was continued for 6 hrs. Cooling at room temperature, the precipitate was filtered. After washing it with the mix solvent (hexane and ethyl acetate) a light yellow colour solid was obtained, characterized by ¹H NMR (Fig. S1) and ¹³CNMR (Fig. S2). ¹H NMR (in DMSO-d₆) (δ , ppm): 9.24 (d, 1H, -CH), 8.50-8.47 (m, 1H, -ArH), 8.26-8.23 (1H, m, -ArH), 8.02 (1H, d, -ArH), 7.75-7.72 (1H, m, -ArH), 7.63-7.60 (1H, m, -ArH), 7.53-7.50 (1H, m, -ArH), 4.34 (q, 2H, -CH₂), 1.37 (t, 3H, -CH₃). ¹³CNMR (in DMSO-d₆) (δ , ppm): 162.8, 155.9, 155.0, 143.7, 135.9, 129.6, 128.9, 126.3, 122.0, 116.4, 111.7, 61.2, 14.0.

Step-2: Synthesis of 3-Oxo-3H-benzo[f]chromene-2-carboxylic acid hydrazide (BCM)

The compound obtained from step-1 was dissolved in 20 ml of ethanol (5 mmol, 1.34 g) and hydrazine hydrate was added in equimolar ratio (5 mmol) under refluxing condition for 6 h. A yellow solid was formed during the reaction. The product BCM was collected and analyzed by ¹H NMR (Fig. S3), ¹³C NMR (Fig. S4)

and Mass spectrum (Fig. S5). ESI-MS⁺ (m/z): 277 (BCM + Na⁺), ¹H NMR (in DMSO-d₆) (δ , ppm): 9.68 (1H, s, -CH), 9.39 (1H, s, -NH), 8.58 (1H, d, -ArH), 8.31 (1H, d, -ArH), 8.09 (1H, d, -ArH), 7.79 (1H, t, -ArH), 7.69-7.63 (2H, m, -ArH), 4.79 (2H, m, -NH₂). ¹³C NMR (in DMSO-d₆) (δ , ppm): 160.2, 159.7, 154.0, 141.7, 135.4, 129.9, 128.9, 128.8, 126.5, 122.2, 117.5, 116.3, 112.6

Physical Instrumentations and Experimental Methods

The descriptions of instruments used in experiment, preparation of solution, experimental methods to carry out this work are supplied in the **Supporting Information**.

CONCLUSION

In brief, we are reporting herewith a smart fluorescent probe BCM on benzocoumarin platform which selectively recognises NO under physiological conditions. From the linear F.I. vs. [NO] plot obtained from fluorescence titration experiment gives $K_f = (4.33 \pm 0.48) \times 10^4 \text{ M}^{-1}$. Here, the acid-hydrazide moiety of probe BCM reacts with NO/O₂ to form electron deficient 1,2,3,4-oxatriazole moiety which is solely responsible for fluorescence enhancement through PET blocking mechanism. The outstanding sensing performance of BCM towards NO is also illustrated by its very low detection limit (16 nM), specific response to NO with desirable selectivity and sensitivity in the presence of other biological reactive species which makes the probe highly potent for NO detection in biological environment. The reaction mechanism of BCM and NO was confirmed by kinetic studies which reveals a 1st order dependence on BCM and 2nd order on NO. The pH variation study in NO detection also supports BCM as an efficient NO sensor in a wide range of pH. Beside these, the bio-imaging implication of this probe is also appreciable owing to its least cytotoxicity, bio compatibility for *in vitro* NO detection. The application of BCM can also be extended to flow cytometric analysis of exogenous and endogenous NO in living cells. So, all the above-mentioned experiments and information certify BCM as a very appropriate probe for the tracking of NO.

Conflicts of interest

There are no conflict of interest to declare

ACKNOWLEDGMENTS

Financial support from DST (Ref. No. 809(Sanc)/ST/P/ S&T/4G-9/2104) West Bengal and CSIR (Ref. 01(2896)/17/EMR-II), New Delhi, India, is gratefully acknowledged. D. Maiti is grateful to DST-INSPIRE for the fellowship (SRF).

REFERENCES

- (a) P. F. Bove and A. D. V. Vliet, *Free Radical Biol. Med.*, 2006, **41**, 515–527. (b) A. H. Ashoka, F. Ali, R. Tiwari, R. Kumari, S. K. Pramanik, and A. Das, *ACS Omega.*, 2020, **5**, 1730–1742.
- D. J. Stuehr, J. Santolini, Z. Q. Wang, C. C. Wei and S. Adak, *J. Biol. Chem.*, 2004, **279**, 36167–36170.
- (a) P. Pacher, J. S. Beckman and L. Liaudet, *Physiol. Rev.*, 2007, **87**, 315–424. (b) Y. Liu, H. Fan, Y. Wen, T. Jia, Q. Su, and F. Lia, *Dyes Pigm.* 2019, **166**, 211–216.
- A. De Mel, F. Murad and A. M. Seifalian, *Chem. Rev.*, 2011, **111**, 5742–5767.
- Y. Iwakiri and M. Y. Kim, *Trends Pharmacol. Sci.*, 2015, **36**, 524–536.
- S. P. Hussain, L. J. Hofseth and C. C. Harris, *Nat. Rev. Cancer.*, 2003, **3**, 276–285.
- B. V. Khan, D. G. Harrison, M. T. Olbrych, R. W. Alexander and R. M. Medford, *Proc. Natl. Acad. Sci. U. S. A.*, 1996, **93**, 9114–9119.
- K. Pantopoulos and M. W. Hentze, *Proc. Natl. Acad. Sci. U. S. A.*, 1995, **92**, 1267–1271.
- (a) B. J. Privett, J. H. Shin and M. H. Schoenfish, *Chem. Soc. Rev.*, 2010, **39**, 1925–1935. (b) S. Biswas, Y. Rajesh, S. Barman, M. Bera, A. Paul, M. Mandal and N. D. P. Singh *Chem. Commun.*, 2018, **54**, 7940–7943.
- S. R-Nuévalos, M. Parra, S. Ceballos, S. Gil and A. M. Costero, *J. Photochem. Photobiol. A*, 2020, **388**, 112132.
- (a) E. Sasaki, H. Kojima, H. Nishimatsu, Y. Urano, K. Kikuchi, Y. Hirata and T. Nagano, *J. Am. Chem. Soc.*, 2005, **127**, 3684–3685. (b) Z. Yu, J. Zhou, X. Dong, W. Zhao and Z. Chen, *Anal. Chim. Acta*, 2019, **1067**, 88–97.
- Y. Yang, S. K. Seidlits, M. M. Adams, V. M. Lynch, C. E. Schmidt, E. V. Anslyn and J. B. Shear, *J. Am. Chem. Soc.*, 2010, **132**, 13114–14116.
- L. E. McQuade and S. J. Lippard, *Inorg. Chem.*, 2010, **49**, 7464–7471.
- M. H. Lim and S. J. Lippard, *Inorg. Chem.*, 2004, **43**, 6366–6370.
- L. Y. Niu, Y. Z. Chen, H. R. Zheng, L. Z. Wu, C. H. Tung and Q. Z. Yang, *Chem. Soc. Rev.*, 2015, **44**, 6143–6160.
- M. Gao, F. Yu, C. Lv, J. Choo and L. Chen, *Chem. Soc. Rev.* 2017, **46**, 2237–2271.
- N. Zhang, Y. Si, Z. Sun, L. Chen, R. Li, Y. Qiao and H. Wang, *Anal. Chem.*, 2014, **86**, 11714–11721.
- F. Yu, P. Li, G. Zhao, T. Chu and K. Han, *J. Am. Chem. Soc.*, 2011, **133**, 11030–11033.
- G. Chen, Q. Fu, F. Yu, R. Ren, Y. Liu, Z. Cao, G. Li, X. Zhao, L. Chen, H. Wang and J. You, *Anal. Chem.*, 2017, **89**, 8509–8516.
- (a) W. Hu, D. Boateng, J. Kong and X. Zhang, *Austin J. Biosens. Bioelectron.*, 2015, **1**, 1–9. (b) T. Zhou, J. Wang, J. Xu, C. Zheng, Y. Niu, C. Wang, F. Xu, L. Yuan, X. Zhao, L. Liang and P. Xu *Anal. Chem.*, 2020, **92**, 5064–5072.
- (a) C. J. Reinhardt, E. Y. Zhou, M. D. Jorgensen, G. Partijilo and J. Chan, *J. Am. Chem. Soc.*, 2018, **140**, 1011–1018. (b) Y. Huo, J. Miao, J. Fang, H. Shi, J. Wang and W. Guo, *Chem. Sci.*, 2019, **10**, 145–152.
- (a) C. Xu, C. Xin, C. Yu, M. Wu, J. Xu, W. Qin, Y. Ding, X. Wang, L. Li and W. Huang, *Chem. Commun.*, 2018, **54**, 13491–13494. (b) X. Lv, Y. Wang, S. Zhang, Y. Liu, J. Zhang and W. Guo, *Chem. Commun.*, 2014, **50**, 7499–7502.
- M. H. Lim and S. J. Lippard, *J. Am. Chem. Soc.*, 2005, **127**, 12170–12171.
- D. A. Jose, N. Sharma, R. Sakla, R. Kaushik and S. Gadiyaram, *Methods*, 2019, **168**, 62–75
- A. S. M. Islam, M. Sasmal, D. Maiti, A. Dutta, S. Ganguly, A. Katarkar, S. Gangopadhyay and M. Ali, *ACS Appl. Bio Mater.*, 2019, **2**, 1944–1955.
- D. Maiti, A. S. M. Islam, M. Sasmal, C. Proadhan and M. Ali, *Photochem. Photobiol. Sci.*, 2018, **17**, 1213–1221.
- (a) A. Dutta, A. S. M. Islam, D. Maiti, M. Sasmal, C. Proadhan and M. Ali, *Org. Biomol. Chem.*, 2019, **17**, 2492–2501. (b) P. Srivastava, M. Verma, S. Sivakumar, and A. K. Patra, *Sens. Actuators B Chem.*, 2019, **291**, 478–484.
- X. Zhang, B. Wang, Y. Xiao, C. Wang and L. He, *Analyst*, 2018, **143**, 4180–4188.
- X.-X. Chen, L.-Y. Niu, N. Shao and Q.-Z. Yang, *Anal. Chem.*, 2019, **91**, 4301–4306.
- A. Beltrán, M. Isabel Burguete, D. R. Abánades, S. D. Pérez-Sala, V. Luis and F. Galindo, *Chem. Commun.*, 2014, **50**, 3579–3581.
- Q. Wang, X. Jiao, C. Liu, S. He, L. Zhaoab and X. Zeng, *J. Mater. Chem. B.*, 2018, **6**, 4096–4103.
- S.-J. Li, D.-Y. Zhou, Y. Li, H.-W. Liu, P. Wu, J. Ou-Yang, W.-L. Jiang and C.-Y. Li, *ACS Sens.*, 2018, **3**, 2311–2319.
- (a) C. Sun, W. Shi, Y. Song, W. Chen and H. Ma, *Chem. Commun.*, 2011, **47**, 8638–8640. (b) A. V. Latha, M. Ayyappan, A. R. Kallar, R. V. Kakkadavath, S. P. Victor and S. Selvam, *Mater. Sci. & Eng. C.*, 2020, **108**, 110463.
- (a) A. S. M. Islam, R. Bhowmick, B. C. Garain, A. Katarkar and M. Ali, *J. Org. Chem.* 2018, **83**, 13287–13295. (b) C. M. Wu, Y. H. Chen, K. Dayananda, T. W. Shiue, C. H. Hung, W. F. Liaw, P. Y. Chen, Y. M. Wang, *Anal. Chim. Acta*, 2011, **708**, 141–148. (c) M. E. Azab, H. M. F. Madkour, M. A. E. Ibraheem, *Phosphorus, Sulfur Silicon Relat. Elem.* 2006, **181**, 1299–1313. (d) M. K. Ibrahim, K. El-Adl, M. F. Zayed and H. A. Mahdy, *Med. Chem. Res.* 2015, **24**, 99–114.
- (a) H. Ammar, S. Fery-Forgues, R. El. Gharbi, *Dyes Pigments.*, 2003, **57**, 259. (b) S. Sastry, *Biophys. Chem.* 2001, **91**, 191. (c) M. Chiyomi, M. Toshinobu, K. Yasuko, T. Kenichiro, Y. Hideyuki, N. Hitoshi, Y. Masatoshi, and T. Akira, *Chem. Pharm. Bull.*, 2005, **53**, 750.
- (a) M. A. Saleh, A. Kamel, A. El-Demerdash and J. Jones, *Chemosphere.*, 1998, **36**, 1543–1552. (b) H. Yu, H. Mizufune, K. Uenaka, T. Moritoki and H. Koshima, *Tetrahedron Lett.*, 2005, **61**, 8932–8938. (c) S. Xiao, T. Yi, F. Li and C. Huang, *Tetrahedron Lett.*, 2005, **46**, 9009–9012.

37. M. Walshe, J. Howarth, M. T. Kelly, R. O'Kennedy and M. R. Smyth, *J. Pharm. Biomed. Anal.*, 1997, **16**, 319-325.
38. (a) B. Kovac and I. Novak, *Spectrochim. Acta, Part A: Mol. Biomol. Spectrosc.*, 2002, **58**, 1483. (b) B. A. Elsayeda, I. A. Ibrahema, M. S. Attia, S. M. Shaabana and M. M. Elsenety, *Sens. Actuators B Chem.*, 2016, **232** 642-652.
39. (a) R. Zhang, H. Zheng and J. Shen, *Synth. Met.*, 1999, **106**, 157-160. (b) N. Mishra, V. Patil, A. Asrondkar, A. S. Bobade, and A. S. Chowdhary, *World J. Pharm. Res.*, **2015**, **4**, 627-636.
40. (a) J. Preat, D. Jacquemin and E. A. Perpe'te, *Chem. Phys. Lett.*, 2005, **415**, 20-24. (b) R. and H. S. B. Naik, H. N. H. Kumar, K. M. Hosamani and K. M. Mahadevan, *Arkivoc.*, **2009**, ii, 11-19. (c) R. M. Zaki, Y. A. Elossaily, and A. M. Kamal El-Dean, *Russian Journal of Bioorganic Chemistry*, **2012**, **38**, 639-646.
41. A. S. M. Islam, R. Alam, A. Katarkar, K. Chaudhuri and M. Ali, *Analyst*, 2015, **140**, 2979-2983.
42. H. Kojima, N. Nakatsubo, K. Kikuchi, S. Kawahara, Y. Kirino, H. Nagoshi, Y. Hirata and T. Nagano, *Anal. Chem.*, 1998, **70**, 2446-2453.
43. H. Kojima, M. Hirotsu, N. Nakatsubo, K. Kikuchi, Y. Urano, T. Higuchi, Y. Hirata and T. Nagano, *Anal. Chem.*, 2001, **73**, 1967-1973.
44. E. Sasaki, H. Kojima, H. Nishimatsu, Y. Urano, K. Kikuchi, Y. Hirata and T. Nagano, *J. Am. Chem. Soc.*, 2005, **127**, 3684-3685.
45. V. G. Kharitonov, A. R. Sundquist and V. S. Sharma, *J. Biol. Chem.* 1994, **269**, 5881-5883.
46. M. Grätzel, S. Taniguchi and A. Henglein, *Ber. Bunsen-Ges. Phys. Chem.*, 1970, **74**, 488-492.
47. W. R. Licht, S. R. Tannenbaum and W. M. Deen, *Carcinogenesis*, 1988, **9**, 365-372.
48. A. S. M. Islam, R. Bhowmick, K. Pal, A. Katarkar, K. Chaudhuri and M. Ali, *Inorg. Chem.*, 2017, **56**, 4324-4331.
49. T. Chen, R. Zamora, B. Zuckerbraun and T. R. Billiar, *Curr. Mol. Med.*, 2003, **3**, 519-526.